Interparticle magnetic correlations in dense Co nanoparticle assemblies

Jeffrey B. Kortright,[1] Olav Hellwig,[2] Karine Chesnel,[1] Shouheng Sun,[3] and Eric E. Fullerton[2]
[1]*Lawrence Berkeley National Laboratory, Berkeley, California 94720, USA*
[2]*San Jose Research Center, Hitachi Global Storage Technologies, 650 Harry Road, San Jose, California 95120, USA*
[3]*IBM T. J. Watson Research Center, Yorktown Heights, New York 10598, USA*
(Received 21 October 2004; published 4 January 2005)

Resonant magnetic x-ray scattering from dense assemblies of 9-nm-diameter ε-Co and *hcp*-Co superparamagnetic particles is reported. For lower anisotropy ε-Co assemblies remanent scattering is significantly enhanced compared to a random orientation model, indicating that preferred intermoment orientations with antiferromagnetic character exist with spatial frequencies ranging over several nearest neighbors. This interaction-mediated collective behavior is consistent with dipolar energies and exists well into the superparamagnetic regime, revealing that such thermally activated motion is highly correlated.

DOI: 10.1103/PhysRevB.71.012402 PACS number(s): 75.25.+z, 75.20.−g, 75.50.Tt, 75.75.+a

Magnetic nanoparticles with protective organic shells often self-assemble into densely packed arrays[1,2] in which close interparticle spacing increases the dipolar interaction energy between particles to compete with single-particle anisotropy, Zeeman, and thermal energies.[3,4] The magnetostatic energy between dipoles $\boldsymbol{\mu}_i$ and $\boldsymbol{\mu}_j$ separated by $\mathbf{r}_{ij}$, $E^D_{i,j} = (\boldsymbol{\mu}_i \cdot \boldsymbol{\mu}_j)/r^3_{ij} - 3(\boldsymbol{\mu}_i \cdot \mathbf{r}_{ij})(\boldsymbol{\mu}_j \cdot \mathbf{r}_{ij})/r^5_{ij}$, has minima ranging from ferromagnetic (F) alignment when $\boldsymbol{\mu}_i$, $\boldsymbol{\mu}_j$, and $\mathbf{r}_{ij}$ are collinear, to antiferromagnetic (AF) alignment when collinear $\boldsymbol{\mu}_i$ and $\boldsymbol{\mu}_j$ are orthogonal to $\mathbf{r}_{ij}$. Thus orientations taken by interacting dipoles in dense assemblies often involve frustration and spin-glass behavior. The correlation function $\xi = \langle \boldsymbol{\mu}_i \cdot \boldsymbol{\mu}_j \rangle$ is a useful descriptor for the ensemble of local moment correlations, since it has positive and negative extrema for these same collinear F and transverse AF order, respectively.[3] Macroscopic magnetic measurements[5–10] and micromagnetic modeling studies[3,4,11,12] reveal the importance of dipolar interactions that are thought to lead to collective behavior below the blocking temperature (T_B) of otherwise superparamagnetic (SPM) particles.[3,11,6] Few measurements, however, are sensitive to interactions at interparticle length scales, where they should be most pronounced.

In this Brief Report, we use resonant x-ray scattering to observe magnetic structure in dense assemblies of 9 nm Co particles having different anisotropy. We focus on the scattering above T_B where the particles form SPM systems. Neutron scattering has long been used to measure paramagnetic scattering in F and AF solids.[13] A characteristic shift in magnetic scattering away from Bragg peaks into more diffuse paramagnetic distributions is observed as T increases above magnetic ordering temperatures. In these bulk studies, exchange interactions are responsible for the observed interatomic paramagnetic correlations. In the present systems, only dipolar interparticle interactions exist to mediate the SPM correlations.

We isolate magnetic from charge scattering via field-dependent measurements and observe it to shift to lower spatial frequencies in the SPM remanent state relative to its saturated distribution. We develop a kinematical scattering model to understand how this SPM scattering is influenced by dipolar interactions and conclude that the remanent SPM scattering from the higher anisotropy sample is consistent with randomly oriented moments. The lower anisotropy sample, however, shows strongly enhanced SPM scattering indicating that statistically significant dipolar interactions having AF character exist out to several particle diameters. The results show directly that dipolar interactions can strongly influence time-averaged interparticle magnetic order even well above T_B of the individual particles.

Densely packed arrays were formed from hexane dispersions of 9-nm-diameter (±5%) Co particles of the cubic, lower anisotropy, ε phase[14] and higher anisotropy *hcp* phase.[15] The samples were prepared by allowing drops of suspended particles to dry on 150 nm thick Si_3N_4 membranes for transmission measurements. Macroscopic magnetic properties were studied with superconducting quantum interference device (SQUID) magnetometry and ac susceptibility. Interparticle properties were obtained from the scattered intensity $I(q,H)$ measured in symmetric transmission geometry [Fig. 1(b) inset] to position the scattering vector $\mathbf{q}$ in the membrane plane,[16] using both linear (I_{lin}) and circular ($I_{\pm}$) polarization with variable applied field $\mathbf{H}$ perpendicular to the membrane at 298 K. Several samples of each phase were observed to have similar behavior; here we present detailed results from one sample of each phase.

Magnetometry, ac susceptibility, and x-ray measurements verify SPM assemblies at 298 K for the relevant time scale of x-ray measurements. Hysteresis loops show no coercivity. Zero-field cooled measurements of magnetization (M) vs increasing T peak at the frequency dependent T_B well below 298 K. In the x-ray measurements, each 50 ps synchrotron pulse yields an intensity snapshot of a particular ensemble of moment orientations that are blocked at this time scale. However, the relevant x-ray measurement time $\tau_M (\sim 10^2 - 10^3$ s) integrates over many snapshots to yield a time average of various particle moment configurations if particles are thermally activated. ac susceptibility in the $1-10^3$ Hz range exhibits T peaks that extrapolate the time-dependent $T_B = E_A/[k \ln(\tau_M/\tau_0)]$ to ~ 200 K for τ_M in this range, where E_A is the activation energy and τ_0 the attempt frequency.

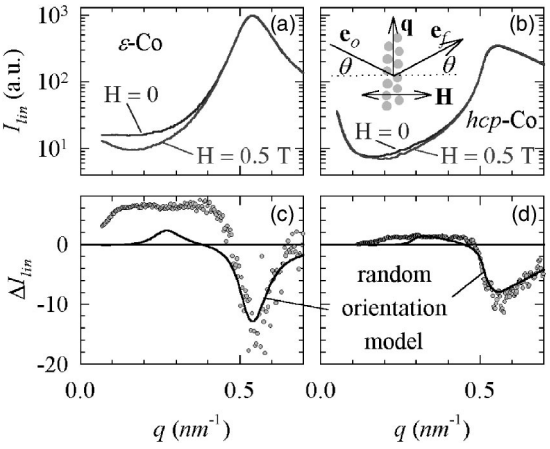

FIG. 1. (Color online) (a) and (b) show q-resolved intensities for the ε- and *hcp*-Co samples measured with linear polarization at saturation and remanence. Inset in (b) is a schematic of the scattering geometry ($\mathbf{q}\|\mathbf{z}, \mathbf{H}\|\mathbf{x}$). (c) and (d) show the field-dependent difference (symbols) for the samples above, and predictions (lines) based on a model of randomly oriented, noninteracting particles described in the text.

Spatially averaging transmission absorption measurements across the Co $L_{2,3}$ edges in a near saturating field, $H_{sat}=\pm 0.5$ T, using circular polarization yields the imaginary parts, f_2, of the resonant magnetic (f_m) and charge (f_c) atomic scattering factors $f_{m/c}=f_{1,m/c}+if_{2,m/c}$,[17,18] seen for ε-Co in Fig. 2. The real parts, f_1, are obtained via Kramers-Kronig transformation. Calculated intensity spectra of pure magnetic and charge scattering are in the inset; $|f_m|^2/|f_c|^2 = 0.026$ for ε-Co at the L_3 line, where data below were collected. Similar spectra for the *hcp*-Co sample yield slightly larger f_c and f_m values at the L_3 peak and intensity ratio 0.037. The absorption step in $f_{2,m}$ indicates that aggregated regions are $\sim 5-10$ particles thick. The strength of the $f_{2,c}$ lines are comparable to those in bulk Co.[19] The size of $f_{2,m}$ relative to $f_{2,c}$ lines is 2 to 3 times smaller than for bulk Co, so the average moment per atom in the particles is correspondingly smaller ($\sim 0.5-0.8\ \mu_B$ vs $1.7\ \mu_B$ in bulk Co). A 9 nm particle contains $\sim 34\,000$ atoms, and so has moment $|\boldsymbol{\mu}| \sim 22\,000\ \mu_B$.

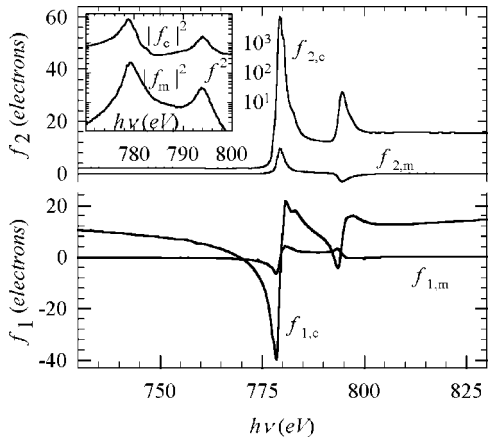

FIG. 2. (Color online) Real (f_1) and imaginary (f_2) parts of the charge and magnetic scattering factors for the ε-Co sample are in the top and bottom panels, respectively. The inset shows the relative strengths of pure charge and magnetic scattering intensities.

Interparticle chemical structure is obtained from $I_{lin}(q)$ for the ε- and *hcp*-Co samples [Figs. 1(a) and 1(b)]. Each sample exhibits a diffuse ring at $q_{peak}=0.54\ \text{nm}^{-1}$ arising from interparticle interference. These data are normalized for slit size effects and by the spherical particle form factor. The characteristic length $2\pi/q_{peak}=11.6$ nm confirms dense assemblies, and that the organic ligand shells remain intact. The peak widths $\Delta q=0.096$ and $0.12\ \text{nm}^{-1}$ for the ε- and *hcp*-Co samples, respectively, suggest relatively disordered particle assemblies, and the different peak shapes reveal measurable differences in interparticle microstructure in the two samples. The *hcp* sample exhibits increasing intensity as $q \to 0$ indicating inhomogeneity at length scales >500 nm.

Magnetic structural information is obtained from the difference between q scans measured at $H=0$ and H_{sat}. For each sample, $I_{lin}(H=0)$ is systematically smaller than $I_{lin}(H_{sat})$ at q_{peak}, and larger at lower q, reminiscent of neutron scattering from paramagnetic solids. These general differences $\Delta I_{lin} \equiv I_{lin}(H=0)-I_{lin}(H_{sat})$ [Figs. 1(c) and 1(d)] are clearly magnetic in origin, and are simply understood qualitatively. At H_{sat} all $\boldsymbol{\mu}_i$ lie along $\mathbf{H}$, yielding commensurate charge and magnetic scattering amplitudes for which magnetic intensity adds to the charge intensity at q_{peak} and for all q. Thermal activation at $H=0$ reduces the commensurate magnetic intensity at q_{peak}, and yields increased SPM scattering at lower q. A quantitative scattering model is developed to understand if and how dipolar interactions contribute to this SPM scattering.

Sensitivity to the orientation of individual $\boldsymbol{\mu}_i$ is given by the atomic scattering factor $f=p_c f_c+p_m f_m$, where $p_c=(\mathbf{e}_f^*\cdot\mathbf{e}_0)$ and $p_m=-i(\mathbf{e}_f^*\times\mathbf{e}_0)\cdot\mathbf{m}$ are the charge and magnetic polarization prefactors depending on scattering angle 2θ, incident and final polarizations $\mathbf{e}_0$ and $\mathbf{e}_f$, and magnetization direction $\mathbf{m}\equiv\boldsymbol{\mu}/|\boldsymbol{\mu}|$.[17] The scattering geometry used is overwhelmingly sensitive to the longitudinal ($\|\mathbf{x}$) projection of moments, be they static or thermally activated. Furthermore, we are sensitive to structure with $\mathbf{r}_{ij}\|\mathbf{q}$ that is orthogonal to longitudinal $\mathbf{m}$, and hence only to the first term in E_D favoring negative ξ (AF alignment). Using the circular polarization basis with small θ and longitudinal $\mathbf{m}$ gives $f_\pm \cong f_c \mp i f_m$ for opposite helicity.[16]

The scattered intensity from interfering particles in the Born approximation can then be written

$$I_\pm(q,\omega,H) = f_c^2 s_{c-c} + f_m^2 s_{m-m} \pm 2(f_{2c}f_{1m} - f_{1c}f_{2m})s_{c-m}, \quad (1)$$

where $\pm$ subscripts refer to right and left circular polarization, and partial structure factors $s_{c-c}(q)$, $s_{m-m}(q,H,\omega)$, and $s_{c-m}(q,H,\omega)$ describe the spatial distribution of charge-charge, magnetic-magnetic, and charge-magnetic correlations, respectively. The q-dependent spherical particle form factor is not explicitly included, as the data have already been normalized by it. p_c and p_m are implicit in the s_{i-j}, so that any temporal fluctuations of $\mathbf{m}_i$ yield frequency (ω) dependence only in s_{m-m} and s_{c-m}. Since s_{c-m} and s_{m-m} are odd and even in helicity, respectively, it follows that $I_+ - I_-$

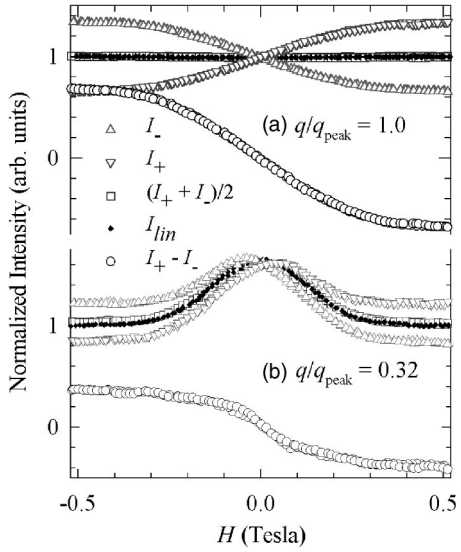

FIG. 3. (Color online) Scattering hysteresis loops at indicated q values using linear and opposite circular polarization for the ε-Co sample. Also shown are the average and difference of opposite circular loops. Data are normalized so that I_{lin} and $(I_+ + I_-)/2$ equal 1 at saturation.

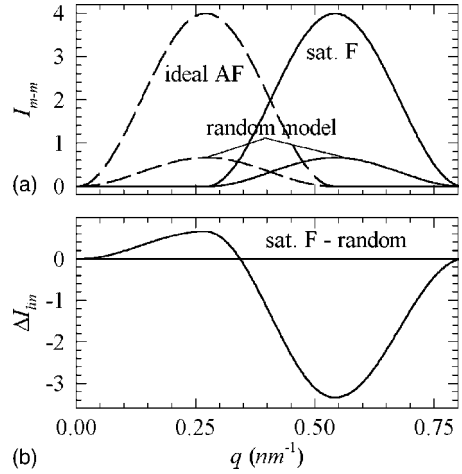

FIG. 4. (Color online) Model calculations (top) of pure magnetic intensity for saturated longitudinal ferromagnetic (F) alignment and ideal longitudinal antiferromagnetic (AF) alignment. Randomly oriented particles would have an equal probability (1/6) of AF and F alignment with magnetic scattering equal to the sum of the two reduced curves. Subtracting the saturated stated from the random state gives a difference curve (bottom) with characteristic AF and F peaks.

$=4(f_{2c}f_{1m}-f_{1c}f_{2m})s_{c-m}$ gives only the cross-term, as noted in Ref. 20, and that $I_{lin} \equiv (I_+ + I_-)/2 = f_c^2 s_{c-c} + f_m^2 s_{m-m}$.

Confirmation of this scattering model comes from hysteresis loops of I_+, I_-, and I_{lin} measured at $q/q_{peak}=1.0$ and 0.32 for the ε-Co sample shown in Fig. 3. The identity $I_+ + I_- \equiv 2I_{lin}$, its second order dependence on M and helicity, and the first order dependence of $I_+ - I_-$ hold for all q values and for both samples. We see that the field dependence of I_{lin}, rather than $I_+ - I_-$, is most appropriate to study dipolar interactions that manifest through the interference of magnetic amplitudes. The SPM scattering in $\Delta I_{lin}(q)$ is seen as a pronounced remanent peak in the loops at $q/q_{peak}=0.32$, while the loss at $q/q_{peak}=1.0$ is within the size of the data symbols since it sits atop the much larger charge peak. Thermal activation is confirmed for both samples from the lack of remanence or coercivity in these loops.

We apply this theory by considering $s_{m-m}(q)$ evaluated for several idealized magnetic configurations for a simple linear lattice of particles oriented along **q**. This lattice extends for just six particles to yield peak widths comparable to those measured. The saturated magnetic configuration yields a peak in $s_{m-m}(q)$ at the same q_{peak} as the $s_{c-c}(q)$ charge peak [Fig. 4(a)]. A hypothetical, ideal AF superlattice with all $\mathbf{m}_i \| \mathbf{x}$ and adjacent $\mathbf{m}_i \cdot \mathbf{m}_j = -1$ yields a peak of the same width and intensity at $q_{peak}/2$ [also in Fig. 4(a)]. Next, consider a model in which each $\mathbf{m}_i$ takes all orientations with equal probability, independent of $\mathbf{m}_{j \neq i}$, to describe a noninteracting SPM assembly. At any given time, nearest neighbors are equally likely to have F or AF alignment with respect to each other, and integrating over $\mathbf{m}_i$ orientations gives peaks at q_{peak} and $q_{peak}/2$, each with 1/6 the intensity of the saturated and ideal AF peaks, respectively, also shown in Fig. 4(a). Evaluating ΔI_{lin} for this hypothetical, noninteracting remanent SPM configuration yields the difference curve in Fig. 4(b), which captures the main features of the measured results in Figs. 1(c) and 1(d), namely the pronounced negative peak at q_{peak} and positive peak near $q_{peak}/2$. The positive $\frac{1}{2}$ order peak results from the longitudinal projections of nearest neighbor **m** pairs that have AF character. These moments need not be rigidly AF coupled to yield this scattering, but simply must have an AF longitudinal projection at some point in their uncorrelated thermally activated motion.

In comparing measured ΔI_{lin} with this noninteracting random orientation model, we can improve on its idealized lattice since we know that both $s_{c-c}(q)$ and $s_{m-m}(q, H_{sat}) \propto I_{lin}(q, H_{sat})$ for each sample, i.e., we know the shape of $s_{m-m}(q, H_{sat})$. Generalizing the random orientation model using sample-specific frequency spectra yields the lines in Figs. 1(c) and 1(d), which have been scaled to the measured first order peak. For the *hcp* sample, the agreement between the model and measured ΔI_{lin} is remarkably good. We conclude that, at least for longitudinal moment projections, dipolar interactions are not sufficient to become evident in the scattering and that the particle moment orientations are random for this sample.

The SPM ε-Co sample scatters significantly more strongly at low q than predicted for noninteracting, randomly oriented particles, not only near $q_{peak}/2$ but extending with roughly constant intensity down to $\sim q_{peak}/5$. Given our predominant sensitivity to longitudinal **m**, the internal reference to the longitudinal saturated state, and the prediction of well-defined AF scattering from the random-orientation model, it is clear that the strong positive feature in ΔI_{lin} for ε-Co must originate from longitudinal AF correlations enhanced by dipolar interactions. For example, if the AF dipolar term in E_D were to influence thermally activated nearest neighbors to favor AF correlations, this would increase the intensity of the $q_{peak}/2$ peak relative to the first order peak, but this alone

would not broaden the $\frac{1}{2}$ order peak. One explanation for its increased width would be that the AF correlations have a smaller coherence length, on average, than that of the particle assembly. This would both broaden and diminish strength of the $\frac{1}{2}$ order peak whose position would remain at $q_{peak}/2$.

To summarize our conclusions, the scattering from the *hcp* assembly is consistent with randomly oriented, uncorrelated longitudinal moments, while that from the ε-Co sample shows strongly enhanced AF correlations over a broad range. Considering the time-average nature of these measurements, it is clear that these correlations are maintained during the thermally activated motion of individual particles. In other words, a correlated or collective state exists above T_B for this sample. Neither sample exhibits a strong remanent magnetic peak well below the $\frac{1}{2}$ order position, where we would expect a peak from domains extending for many particles in the sample plane,[21] leading us to conclude that such domains are not present in these samples.

We interpret the pronounced differences in remanent magnetic structure between the two samples as resulting from several sources. The average moment and anisotropy of individual particles are different in the ε and *hcp* phase particles. This in turn leads to differences in the relative magnitudes of the anisotropy and dipolar energy densities in the two assemblies. It is reasonable to assume that the ratio of anisotropy to dipolar energies is larger in the *hcp* sample; this coupled with a random distribution of anisotropy axes would yield a more uncorrelated remanent state for the *hcp* assembly, as observed. The dipolar energy and magnetic structure are known to depend sensitively on precise details of the three-dimensional interparticle order, which is different for the two samples as indicated in their different shapes of $I_{lin}(q, H_{sat})$. Thus microstructural differences between the two assemblies are expected to contribute to the different remanent magnetic spectra, in addition to differences in isolated particle properties.

These first resonant soft x-ray measurements of interparticle magnetic structure in particle assemblies reveal high sensitivity, even down to the particle monolayer level. This ability to measure interparticle magnetic structure will become increasingly important as assemblies with controlled microstructures, and as new types of magnetic cluster assemblies, emerge.

Measurements were made at beamlines 8.0 and 4.0 at the Advanced Light Source at LBNL. Work at LBNL was supported by the Director, Office of Science, Office of Basic Energy Sciences, under DOE Contract No. DE-AC03-76SF00098.

[1] S. Sun, C. B. Murray, D. Weller, L. Folks, and A. Moser, Science **287**, 1989 (2000).
[2] V. F. Puntes, K. M. Krishnan, and A. P. Alivisatos, Science **291**, 2115 (2001).
[3] J. L. Dormann, D. Fiorani, and E. Tronc, Adv. Chem. Phys. **98**, 283 (1997).
[4] R. W. Chantrell, N. Walmsley, J. Gore, and M. Maylin, Phys. Rev. B **63**, 024410 (2000).
[5] W. Luo, S. R. Nagel, T. F. Rosenbaum, and R. E. Rosensweig, Phys. Rev. Lett. **67**, 2721 (1991).
[6] T. Jonsson, P. Svedlindh, and M. F. Hansen, Phys. Rev. Lett. **81**, 3976 (1998).
[7] P. Poddar, J. L. Wilson, H. Srikanth, D. F. Farrell, and S. A. Majetich, Phys. Rev. B **68**, 214409 (2003).
[8] G. A. Held, G. Grinstein, H. Doyle, S. Sun, and C. B. Murray, Phys. Rev. B **64**, 012408 (2001).
[9] H. Mamiya, I. Nakatani, and T. Furubayashi, Phys. Rev. Lett. **82**, 4332 (1999).
[10] Y. Sun, M. B. Salamon, K. Garnier, and R. S. Averback, Phys. Rev. Lett. **91**, 167206 (2003).
[11] J.-O. Andersson, C. Djurberg, T. Jonsson, P. Svedlindh, and P. Nordblad, Phys. Rev. B **56**, 13 983 (1997).
[12] J. Garcia-Otero, M. Porto, J. Rivas, and A. Bunde, Phys. Rev. Lett. **84**, 167 (1999).
[13] C. G. Shull, W. A. Strauser, and E. O. Wollan, Phys. Rev. **83**, 333 (1951); M. K. Wilkinson and C. G. Shull, *ibid.* **103**, 516 (1956).
[14] C. B. Murray, S. Sun, H. Doyle, and T. Betley, MRS Bull. **26**, 985 (2001).
[15] S. Sun and C. B. Murray, J. Appl. Phys. **85**, 4325 (1999).
[16] J. B. Kortright, S.-K. Kim, G. P. Denbeaux, G. Zeltzer, K. Takano, and E. E. Fullerton, Phys. Rev. B **64**, 092401 (2001).
[17] J. P. Hannon, G. T. Trammell, M. Blume, and D. Gibbs, Phys. Rev. Lett. **61**, 1245 (1988).
[18] J. B. Kortright and S. K. Kim, Phys. Rev. B **62**, 12 216 (2000).
[19] C. T. Chen, Y. U. Idzerda, H.-J. Lin, N. V. Smith, G. Meigs, E. Chaban, G. H. Ho, E. Pellegrin, and F. Sette, Phys. Rev. Lett. **75**, 152 (1995).
[20] R. M. Osgood III, S. K. Sinha, J. W. Freeland, Y. U. Idzerda, and S. D. Bader, J. Magn. Magn. Mater. **198**, 698 (1999).
[21] V. F. Puntes, P. Gorostiza, D. M. Aruguete, N. G. Bastus, and A. P. Alivisatos, Nat. Mater. **3**, 263 (2004).